

Theory of an electron asymmetric scattering on skyrmion textures in two-dimensional systems

K.S. Denisov*

Ioffe Institute, 194021 St.Petersburg, Russia

(Dated: March 2, 2020)

Abstract

We discuss in details the electron scattering pattern on skyrmion-like magnetic textures in two-dimensional geometry. The special attention is focused on analyzing the scattering asymmetry, which is a precursor of the topological Hall effect. We present analytical results valid for the limiting regimes of strong and weak coupling, we also describe the numerical scheme that gives access to the exact solution of the scattering problem. Based on the numerical computations we investigate the properties of the asymmetric scattering for an arbitrary magnitude of the interaction strength and the topology of a magnetic texture. We analyze in details the conditions when the topological charge of a magnetic texture is indeed essential for the appearance of the Hall response. We also describe how the electron scattering asymmetry is modified due to an additional short-range impurity located inside a magnetic skyrmion.

arXiv:2002.12829v1 [cond-mat.mes-hall] 28 Feb 2020

* denisokonstantin@gmail.com

I. INTRODUCTION

Rapidly growing physics of the topological magnetic textures [1–4] pays a special attention to the emerging nontrivial electrodynamics [5–7] and to the topological Hall effect (THE) in particular. Introduced originally to describe the Hall effect in a skyrmion lattice [8] and being experimentally evidenced in such systems [9–12], the THE contribution however is not specific to this unique kind of geometry. The recent advances in imaging techniques have revealed different material platforms possessing individual skyrmions with size ranging from sub-100 nm [13–17] down to sub-10 nm [18–20]. While the subsequent transport studies of both the discretized skyrmion geometry [21–23] and the non-regular skyrmion arrays [15, 17, 24–28] in general confirm the presence of THE signatures, the estimation of THE magnitude in these systems is still debated as it can be dramatically modified due to an additional impurity scattering or the nonadiabaticity of a carrier spin motion [29–33]. Furthermore, accounting for a mixed spin-orbital electron dynamics becomes especially important when one reduces the skyrmion size and thus inevitably enters into the clean limit of a ballistic electron motion inside the skyrmion. One common approach capable for analyzing these issues is based on the tight-binding model, there are various simulations of THE for individual magnetic textures [34–38] and skyrmion lattices [39–41]. However, as an alternative and somewhat more flexible description one has recently appealed to the scattering theory [42, 43]. Analyzing an electron scattering pattern has allowed to quantify the renormalization of THE magnitude due to various factors on a unified platform [31, 42, 44] thus revealing a high usefulness of this approach.

In this manuscript we present the comprehensive investigation of the electron scattering on skyrmion-like textures. Our main purpose is to analyze the properties of an asymmetric scattering for an arbitrary coupling strength including weak and strong coupling regimes, as well as to clarify the conditions when the topology of a magnetic texture is essential. Encouraged by experimental indications that skyrmions tend to be captured by structural defects [15, 20] we also analyze how an additional impurity potential affects the Hall response.

The paper is organized as follows. In Sec. II we introduce the framework for the electron scattering on a skyrmion texture. In Sec. III we develop the analytic descriptions for the weak and strong coupling regimes; the numerical scheme is further developed in Sec. IV to address the exact solution of the scattering problem. Based on the numerical calculations

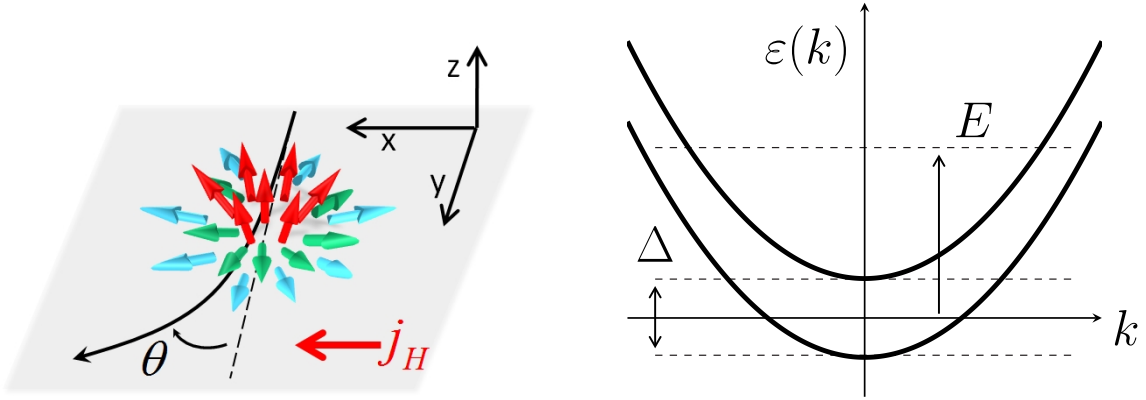


FIG. 1. Electron scattering on a magnetic texture and the electron free motion spectrum.

we analyze various scattering scenarios in Sec. V. In Sec. III B, V B and V D we carefully examine the role of the skyrmion topology on the Hall current. The scattering on electrically charged skyrmions is discussed in Sec. III A and Sec. V C. The scattering features driven by the nonadiabaticity of the electron spin motion can be found in III A, V A.

II. SCATTERING FRAMEWORK

A. Skyrmion scattering potential

We consider a 2D system with the electron Hamiltonian \mathcal{H} given by:

$$\mathcal{H} = \mathcal{H}_0 + V(\mathbf{r}), \quad \mathcal{H}_0 = \frac{\hat{\mathbf{p}}^2}{2m_0} - \frac{\Delta}{2}\sigma_z, \quad (1)$$

here \mathcal{H}_0 describes the electron free motion, m_0 is an effective mass, $\hat{\mathbf{p}}$ is the momentum operator, $\Delta > 0$ is the spin splitting of the electron subbands, the \mathbf{r} -dependent term $V(\mathbf{r})$ is a scattering potential. The spectrum shown in Fig. 1 consists of two parabolas shifted by Δ , the energies are given by $\varepsilon_{\mathbf{k}}^s = \hbar^2 \mathbf{k}^2 / 2m_0 - s\Delta$, where $s = \pm 1/2$ is the electron spin projection onto z axis. There are two regimes with respect to the position of the electron energy E (see Fig. 1), either $E > \Delta/2$ so both spin subbands are available for a free motion, or $E < \Delta/2$ and the propagation in the spin-down subband is suppressed. In what follows we denote the wavevectors at energy E according to the following notation:

$$(E > \Delta/2) \quad k_s = \sqrt{2m_0(E + s\Delta)}, \quad k = \sqrt{2m_0E}. \quad (2)$$

In this paper we consider the scattering potential $V(\mathbf{r})$ of the following form:

$$V(\mathbf{r}) = -g \begin{pmatrix} v_1(r) & u(r)e^{-i(\chi\phi+\gamma)} \\ u(r)e^{i(\chi\phi+\gamma)} & v_2(r) \end{pmatrix}, \quad (3)$$

where $\mathbf{r} = (r, \phi)$, g is a coupling constant, $v_{1,2}(r)$ and $u(r)$ are dimensionless real functions of r only, the parameter $\chi = \pm 1, \pm 2, \dots$ takes integer values, γ is an arbitrary phase. We will assume that the potential has a localized character so that $v_{1,2}, u \rightarrow 0$ at $r \gtrsim r_0$, where r_0 is a localization radius. Of key importance is the dependence of $V(\mathbf{r})$ on the polar angle ϕ entering in its off-diagonal components. The ϕ -dependence leads to the non-commutativity of the Hamiltonian with the operator of angular momentum $-i\partial_\phi$, as a result the electron scattering on $V(\mathbf{r})$ gets an asymmetric character. A comprehensive description of this phenomenon is the main subject of the present paper.

Let us comment on physics underlying the chosen form of $V(\mathbf{r})$. This type of potentials is relevant for magnetic materials when an electron interacts with a single chiral spin texture, such as magnetic skyrmion. Let $\mathbf{n}(\mathbf{r})$ be a unit vector directed along the local magnetization. For an individual chiral spin texture $\mathbf{n}(\mathbf{r})$ can be generally written as:

$$\mathbf{n}(\mathbf{r}) = \left(n_{\parallel}(r) \cos(\chi\phi + \gamma), n_{\parallel}(r) \sin(\chi\phi + \gamma), n_z(r) \right), \quad (4)$$

where (χ, γ) correspond to the vorticity and the helicity of the spin texture, respectively, and $n_{z,\parallel}(r)$ describe the radial profiles (it is assumed that at $r \gtrsim r_0$ one has $n_z \rightarrow 1, n_{\parallel} \rightarrow 0$). The scattering potential $V(\mathbf{r})$ from Eq. 3 appears due to an electron exchange interaction with a static magnetization field of this shape. If no other perturbation is present we can relate g to an exchange interaction constant and the functions $v_{1,2}(r), u(r)$ to the spin profiles:

$$v_1(r) = -v_2(r) = n_z(r) - 1, \quad u(r) = n_{\parallel}(r). \quad (5)$$

The uniform background component outside the texture core $\mathbf{n}(r \gtrsim r_0) = \mathbf{e}_z$ gives rise to the spin subband splitting $\Delta = 2g$ in this case.

We shall mention that when an electron scattering is induced entirely by the perturbation of the magnetization one should assume an additional coupling $v_1 = -v_2$ between the diagonal components of $V(\mathbf{r})$. In what follows, however, we will develop the theory with no restrictions on $v_{1,2}(r)$ functions. By making this generalization we can also introduce to our consideration the possibility of a scalar potential U_0 to be superimposed on a spin texture.

This situation has a great practical interest, as there are numerous experimental observations that skyrmions tend to be pinned by structural defects, i.e. by charged impurities. In particular, the approximation $v_1 \approx v_2$ instead of $v_1 = -v_2$ can be considered to describe the extreme regime with $U_0 \gg g$. The theory present in this work allows us to analyze both these cases.

B. Scattering rates

In this work we treat the scattering problem using the $\hat{T}(z)$ -operator which satisfies the Lippman-Schwinger equation:

$$\hat{T}(z) = V + V\hat{G}_0(z)\hat{T}(z), \quad (6)$$

where $\hat{G}_0(z) = (z - \mathcal{H}_0)^{-1}$ is the Green operator corresponding to the free Hamiltonian, and V corresponds to the scattering potential $V(\mathbf{r})$ defined in Eq. 3. Since $V(\mathbf{r})$ is a 2×2 matrix there are generally 4 scattering channels. To describe an elastic electron scattering with the energy E from (\mathbf{k}', s') to (\mathbf{k}, s) states one deals with the T -matrix on a mass shell:

$$T_{\mathbf{k}\mathbf{k}'}^{ss'} \equiv \lim_{\delta \rightarrow 0} \langle \mathbf{k}s | \hat{T}(E + i\delta) | \mathbf{k}'s' \rangle.$$

The square modulus of so defined T -matrix elements $|T_{\mathbf{k}\mathbf{k}'}^{ss'}|^2$ determine the scattering rates. In particular, the differential scattering cross-section in 2D geometry is defined as [45]:

$$\frac{d\sigma_{ss'}}{d\theta} = \frac{m_0^2}{2\pi\hbar^4 k_{s'}} |T_{\mathbf{k}\mathbf{k}'}^{ss'}|^2, \quad (7)$$

where θ is the scattering angle, i.e. the angle between \mathbf{k} and \mathbf{k}' . In what follows, however, we will describe the scattering using the symmetric $\mathcal{G}_{\mathbf{k}\mathbf{k}'}^{ss'} = \mathcal{G}_{\mathbf{k}'\mathbf{k}}^{ss'}$, and asymmetric $\mathcal{J}_{\mathbf{k}\mathbf{k}'}^{ss'} = -\mathcal{J}_{\mathbf{k}'\mathbf{k}}^{s's}$ dimensionless functions defined as:

$$|T_{\mathbf{k}\mathbf{k}'}^{ss'}|^2 = \frac{1}{\nu_0^2} \left(\mathcal{G}_{\mathbf{k}\mathbf{k}'}^{ss'} + \mathcal{J}_{\mathbf{k}\mathbf{k}'}^{ss'} \right), \quad \nu_0 = \frac{m_0}{2\pi\hbar^2}. \quad (8)$$

Here the prefactor corresponds to the two-dimensional density of states ν_0 . The reason to extract ν_0^2 explicitly from $|T_{\mathbf{k}\mathbf{k}'}^{ss'}|^2$ becomes clear when using the classical description present in III B; it also allows for a compact and natural representation of the Hall resistivity, see the details in Ref. [31].

The asymmetric terms $\mathcal{J}_{\mathbf{k}\mathbf{k}'}^{ss'}$ leading to the Hall response appear due to the intrinsic angular asymmetry of the considered chiral potentials. The integral quantities describing the transverse currents are given by:

$$\mathcal{J}_{ss'} = \int_0^{2\pi} \mathcal{J}_{\mathbf{k}\mathbf{k}'}^{ss'} \sin \theta d\theta. \quad (9)$$

In the following sections we calculate $\mathcal{G}_{\mathbf{k}\mathbf{k}'}^{ss'}$, $\mathcal{J}_{\mathbf{k}\mathbf{k}'}^{ss'}$ and consider the properties of an electron scattering in various regimes and for different potential shapes.

III. ANALYTICAL RESULTS

Let us comment on some general features associated with the scattering on chiral potentials $V(\mathbf{r})$. There are two types of dynamic processes taking place during the electron motion inside the scattering region. Firstly, there is an evolution of its orbital trajectory associated with the change of the momentum in the given potential. Secondly, there is an electron spin rotation driven by its coupling with the spatially non-homogeneous magnetization field. Of highest importance is that these two processes affect each other leading to the appearance of the scattering asymmetry.

In order to develop an *analytical* description for some limiting regimes we should distinguish the role of parameters affecting both orbital and spin motions. For instance, assuming $g = \text{const}$ the magnitude of product kr_0 would determine two orbitally different regimes. Namely, there is the transition from quantum isotropic scattering (described perturbatively) at $kr_0 \lesssim 1$ to the quasiclassical low-angle motion at $kr_0 \gg 1$ governed by the Newton mechanics. The character of an electron spin motion in its turn changes essentially depending on the magnitude of the adiabatic parameter determined as $\lambda_a = \omega_{ex}\tau_{\text{fly}}$, here $\omega_{ex} = 2g/\hbar$ corresponds to the energy difference between spin up and spin down states, and $\tau_{\text{fly}} = (2r_0)/v$ is the time of electron presence inside a texture core, here $v = \sqrt{2E/m_0}$ is the electron velocity. The magnitude of λ_a shows if the electron has enough time for its spin to become adiabatically co-aligned with the local magnetization direction ($\lambda_a \gg 1$), or the perturbation is rather instantaneous ($\lambda_a \lesssim 1$) so that after flying out of the potential region the electron spin only experiences a small rotation with respect to its initial direction. Naturally, the latter scenario $\lambda_a \lesssim 1$ is accompanied by the activation of the spin-flip scattering channels; the adiabatic regime on the contrary is featured by the suppression of the spin-flip processes.

The adiabatic parameter can be written in form $\lambda_a = (2g/E) \cdot (kr_0)$, which indicates that the change of the potential radius r_0 would affect both the orbital and the spin motions at the same moment. As a result it is reasonable to treat the so-called weak coupling regime ($\lambda_a \lesssim 1$) along with the condition $kr_0 \lesssim 1$ on the basis of the perturbation theory, while to consider the opposite adiabatic regime assuming $kr_0 \gg 1$ and using the quasiclassical approximation. Below in this section we present the analytical results for these two limiting regimes. The numerical scheme is further developed in [IV](#) to address the exact solution of the scattering problem.

A. Perturbation theory

In this section we will get analytical expressions for the scattering rates $\mathcal{G}_{\mathbf{k}\mathbf{k}'}^{ss'}$, $\mathcal{J}_{\mathbf{k}\mathbf{k}'}^{ss'}$ using the perturbation theory. We assume $\lambda_a \lesssim 1$ and that the scattering potential has a short-range character, which means that $V(\mathbf{r})$ is nonzero only at $kr_0 \lesssim 1$. The starting point is Eq. [6](#) written for the T -matrix on a mass shell:

$$T_{\mathbf{k}\mathbf{k}'}^{ss'} = V_{\mathbf{k}\mathbf{k}'}^{ss'} + \sum_{\mathbf{g}, s''} \frac{V_{\mathbf{k}\mathbf{g}}^{ss''} T_{\mathbf{g}\mathbf{k}'}^{s''s'}}{E - \varepsilon_{\mathbf{g}}^{s''} + i0}, \quad (10)$$

where E is the electron energy, $\varepsilon_{\mathbf{k}}^s$ is the band spectrum given by Eq. [1](#), and $V_{\mathbf{k}\mathbf{k}'}^{ss'}$ is the matrix element of the scattering potential:

$$V_{\mathbf{k}\mathbf{k}'}^{ss'} = -g \begin{pmatrix} v_1(q) & -ie^{-i(\chi\varphi_q + \gamma)}u(q) \\ -ie^{i(\chi\varphi_q + \gamma)}u(q) & v_2(q) \end{pmatrix}, \quad (11)$$

$$v_{1,2}(q) = 2\pi \int_0^\infty r dr J_0(qr) v_{1,2}(r), \quad u(q) = 2\pi \int_0^\infty r dr J_1(qr) u(r),$$

where $\mathbf{q} = \mathbf{k} - \mathbf{k}' \equiv (q, \varphi_q)$, φ_q is the polar angle of \mathbf{q} , J_0, J_1 are the Bessel functions of zero and first kind respectively (in this section we consider only $\chi = \pm 1$). We are focused on a short-range scattering potential $kr_0 \lesssim 1$, at that one can replace the Bessel functions in the matrix elements Eq. [11](#) by the approximations at small arguments $J_0(x) \approx 1, J_1(x) \approx x/2$:

$$v_{1,2}(q) = 2\pi r_0^2 \cdot \mathcal{I}_{\uparrow, \downarrow}, \quad u(q) = \pi r_0^3 q \cdot \mathcal{I}_{\parallel},$$

$$\mathcal{I}_{\uparrow, \downarrow} = \int_0^1 v_{1,2}(xr_0) x dx, \quad \mathcal{I}_{\parallel} = \int_0^1 u(xr_0) x^2 dx, \quad (12)$$

where the dimensionless numbers $\mathcal{I}_{1,2,\parallel}$ are determined only by particular profiles $v_{1,2}, u$ and have no dependence on r_0 (at least in the limit $kr_0 \lesssim 1$). The q -dependent prefactor in $u(q)$ can be eliminated using the following expression for the exponent $e^{\pm i\varphi_q}$:

$$e^{\pm i\varphi_q} = \frac{1}{q} \left(k e^{\pm i\varphi} - k' e^{\pm i\varphi'} \right), \quad (13)$$

where φ, φ' are the polar angles of \mathbf{k}, \mathbf{k}' respectively.

We firstly consider the regime when both energy branches are available ($\Delta < 2E$). We will also approximate $k_\uparrow \approx k_\downarrow \equiv k$ assuming small spin splitting $\Delta/2E \ll 1$. In the lowest order of the perturbation theory the T -matrix is simply given by the matrix element $T_{\mathbf{k}\mathbf{k}'}^{ss'} = V_{\mathbf{k}\mathbf{k}'}^{ss'}$. The asymmetric rates $\mathcal{J}_{\mathbf{k}\mathbf{k}'}^{ss'}$ are absent in this approximation; the symmetric parts are given by:

$$\begin{aligned} \mathcal{G}_{\mathbf{k}\mathbf{k}'}^{\uparrow\uparrow} &= \left(\frac{g}{2E} \right)^2 (kr_0)^4 \mathcal{I}_\uparrow^2, & \mathcal{G}_{\mathbf{k}\mathbf{k}'}^{\downarrow\downarrow} &= \left(\frac{g}{2E} \right)^2 (kr_0)^4 \mathcal{I}_\downarrow^2 \\ \mathcal{G}_{\mathbf{k}\mathbf{k}'}^{\uparrow\downarrow} &= \mathcal{G}_{\mathbf{k}\mathbf{k}'}^{\downarrow\uparrow} = \left(\frac{g}{2E} \right)^2 (kr_0)^6 \mathcal{I}_\parallel^2 \cdot \sin^2 \theta. \end{aligned} \quad (14)$$

The scattering in the spin-conserving channels is isotropic in analogy with the s -scattering on δ -potential. The scattering in the spin-flip channels, however, acquires an angular dependence featured by the suppression of the forward scattering. Let us mention that the spin-flip scattering rates contain an additional smallness due to the higher order of kr_0 .

We proceed with calculating the asymmetric terms $\mathcal{J}_{\mathbf{k}\mathbf{k}'}^{ss'}$. The second-order correction to the T -matrix is given by:

$$\delta T_{\mathbf{k}\mathbf{k}'}^{ss'} = \sum_{\mathbf{g}, s''} \frac{V_{\mathbf{k}\mathbf{g}}^{ss''} V_{\mathbf{g}\mathbf{k}'}^{s''s'}}{E - \varepsilon_{\mathbf{g}}^{s''} + i0} = \mathcal{P} \sum_{\mathbf{g}, s''} \frac{V_{\mathbf{k}\mathbf{g}}^{ss''} V_{\mathbf{g}\mathbf{k}'}^{s''s'}}{E - \varepsilon_{\mathbf{g}}^{s''}} - i\pi \sum_{\mathbf{g}, s''} \delta(E - \varepsilon_{\mathbf{g}}^{s''}) V_{\mathbf{k}\mathbf{g}}^{ss''} V_{\mathbf{g}\mathbf{k}'}^{s''s'}. \quad (15)$$

The first term in Eq. 15 is the correction to $\mathcal{G}_{\mathbf{k}\mathbf{k}'}^{ss'}$ and we will neglect it (here \mathcal{P} stands for the principal value). The second term gives rise to $\mathcal{J}_{\mathbf{k}\mathbf{k}'}^{ss'}$ via the interference with the first Born approximation terms $V_{\mathbf{k}\mathbf{k}'}^{ss'}$ in the square modulus of T -matrix:

$$\mathcal{J}_{\mathbf{k}\mathbf{k}'}^{ss'} = \nu_0^3 \sum_{s''} \int_0^{2\pi} d\varphi_g \cdot \text{Im} \left[V_{\mathbf{k}\mathbf{g}}^{ss''} V_{\mathbf{g}\mathbf{k}'}^{s''s'} V_{\mathbf{k}'\mathbf{k}}^{s's} \right], \quad (16)$$

here ν_0 is defined in Eq. 8. Indeed, upon the the replacement of the initial (\mathbf{k}', s') and final (\mathbf{k}, s) scattering states the terms $\mathcal{J}_{\mathbf{k}\mathbf{k}'}^{ss'}$ change their signs:

$$\mathcal{J}_{\mathbf{k}\mathbf{k}'}^{ss'} = \nu_0^3 \sum_{s''} \int_0^{2\pi} d\varphi_g \cdot \text{Im} \left[V_{\mathbf{k}\mathbf{g}}^{ss''} V_{\mathbf{g}\mathbf{k}'}^{s''s'} V_{\mathbf{k}'\mathbf{k}}^{s's} \right] = \nu_0^3 \sum_{s''} \int_0^{2\pi} d\varphi_g \cdot \text{Im} \left[\left(V_{\mathbf{g}\mathbf{k}}^{s''s} V_{\mathbf{k}'\mathbf{g}}^{s's''} V_{\mathbf{k}\mathbf{k}'}^{ss'} \right)^* \right] = -\mathcal{J}_{\mathbf{k}'\mathbf{k}}^{s's}.$$

The diagonal matrix elements $V_{\mathbf{k}\mathbf{k}'}^{\uparrow\uparrow}, V_{\mathbf{k}\mathbf{k}'}^{\downarrow\downarrow}$ are real, so the imaginary part of the product 16 is nonzero only for the interference between one spin-conserving and two spin-flip scattering processes, i.e. $\text{Im} \left[V_{\mathbf{k}'\mathbf{k}}^{\uparrow\uparrow} V_{\mathbf{k}g}^{\uparrow\downarrow} V_{g\mathbf{k}'}^{\downarrow\downarrow} \right] \neq 0$ for $(\uparrow\uparrow)$ spin-conserving scattering channel, and $\text{Im} \left[V_{\mathbf{k}'\mathbf{k}}^{\downarrow\downarrow} V_{\mathbf{k}g}^{\uparrow\downarrow} V_{g\mathbf{k}'}^{\downarrow\downarrow} + V_{\mathbf{k}'\mathbf{k}}^{\downarrow\downarrow} V_{\mathbf{k}g}^{\uparrow\uparrow} V_{g\mathbf{k}'}^{\uparrow\downarrow} \right] \neq 0$ for $(\uparrow\downarrow)$ spin-flip scattering channel. Taking into account the explicit forms of $v_{1,2}(q), u(q)$ from Eq. 12 we get finally for $\mathcal{J}_{\mathbf{k}\mathbf{k}'}^{ss'}$:

$$\begin{aligned} \mathcal{J}_{\mathbf{k}\mathbf{k}'}^{\uparrow\uparrow} &= \zeta_{\uparrow} \cdot \sin(\chi\theta), & \mathcal{J}_{\mathbf{k}\mathbf{k}'}^{\downarrow\downarrow} &= -\zeta_{\downarrow} \cdot \sin(\chi\theta), & \mathcal{J}_{\mathbf{k}\mathbf{k}'}^{\uparrow\downarrow} &= \mathcal{J}_{\mathbf{k}\mathbf{k}'}^{\downarrow\uparrow} = \mathcal{J}_{\mathbf{k}\mathbf{k}'}^{\uparrow\uparrow} + \mathcal{J}_{\mathbf{k}\mathbf{k}'}^{\downarrow\downarrow} \\ \zeta_{\uparrow,\downarrow} &= \frac{\pi}{2} \left(\frac{g}{2E} \right)^3 (kr_0)^8 (\mathcal{I}_{\parallel}^2 \cdot \mathcal{I}_{\uparrow,\downarrow}) \end{aligned} \quad (17)$$

Let us discuss the main features of the obtained results. As one naturally expects for a short-range potential the angular dependence of $\mathcal{J}_{\mathbf{k}\mathbf{k}'}^{ss'}$ is determined by the lowest asymmetric angular harmonic of the scattering angle θ , i.e. by the $\sin\theta$. The magnitude of the asymmetric terms scales as the third order of the coupling constant $(g/E)^3$ and more remarkably by the eighth order of $(kr_0)^8$.

It is especially important to analyze the spin-dependent properties of $\mathcal{J}_{\mathbf{k}\mathbf{k}'}^{ss'}$. As follows from Eq. 17 the character of the scattering asymmetry (charge or spin) essentially depends on whether the scattering potential $V(\mathbf{r})$ describes a purely magnetic texture ($v_1 = -v_2$), or it also contains an additional scalar potential ($v_1 \neq -v_2$). Indeed, for a pure chiral spin texture we have $\zeta_{\uparrow} = -\zeta_{\downarrow}$, which leads to the following coupling between $\mathcal{J}_{\mathbf{k}\mathbf{k}'}^{ss'}$:

$$\mathcal{J}_{\mathbf{k}\mathbf{k}'}^{\uparrow\uparrow} = \mathcal{J}_{\mathbf{k}\mathbf{k}'}^{\downarrow\downarrow}, \quad \mathcal{J}_{\mathbf{k}\mathbf{k}'}^{\uparrow\downarrow} = 2\mathcal{J}_{\mathbf{k}\mathbf{k}'}^{\uparrow\uparrow}, \quad (v_1 = -v_2). \quad (18)$$

These relations indicate that the spin-up and spin-down electrons are asymmetrically scattered in the same transverse direction; which one is determined by the product $(\chi \cdot n_z)$. This process leads to the appearance of the Hall current even for totally unpolarized carriers.

On the contrary, if we consider that a strong scalar perturbation is superimposed on a chiral spin texture $U_0 \gg g$ and assume that $v_1 \approx v_2$, the coupling between different scattering channels will take form:

$$\mathcal{J}_{\mathbf{k}\mathbf{k}'}^{\uparrow\uparrow} \approx -\mathcal{J}_{\mathbf{k}\mathbf{k}'}^{\downarrow\downarrow}, \quad \mathcal{J}_{\mathbf{k}\mathbf{k}'}^{\uparrow\downarrow} \approx 0, \quad (v_1 \approx v_2). \quad (19)$$

Thus a strong electron interaction with a nonmagnetic component of the scattering potential leads to the transverse spin current. Moreover, the direction of this current is sensitive to whether the nonmagnetic impurity is positively or negatively charged. In this regard a magnetic skyrmion electrostatic environment can dramatically affect the symmetry properties

of the topological Hall effect and to significantly modify its dependence on a carrier spin polarization.

The spin-dependent structure of the asymmetric scattering can be understood based on the spin chirality arguments. In case of a pure magnetic texture the Hall response is driven by the scalar spin chirality $\mathbf{M}_1 \cdot [\mathbf{M}_2 \times \mathbf{M}_3]$ [46–48] which is irrelevant to the electron spin state; naturally it leads to the spin-independent skew scattering [44]. On the contrary, when the scalar potential is present the scattering asymmetry can be induced due to the mixed product $\mathbf{S} \cdot [\mathbf{M}_2 \times \mathbf{M}_3]$ [32] composing of both the magnetization vector spin chirality $[\mathbf{M}_2 \times \mathbf{M}_3]$ and the electron spin \mathbf{S} , this mechanism thus gives rise to the spin Hall effect.

Let us further consider the case when only one (spin-up) subband is activated ($\Delta > 2E$). The second-order correction to the T -matrix relevant for the scattering asymmetry is written:

$$\delta T_{\mathbf{k}\mathbf{k}'}^{\uparrow\uparrow} = -i\nu_{\uparrow}^2(E) \int_0^{2\pi} d\varphi_g \cdot \nu_{\downarrow}(E) V_{\mathbf{k}\mathbf{g}}^{\uparrow\downarrow} V_{\mathbf{g}\mathbf{k}'}^{\downarrow\uparrow} \quad (20)$$

where $\nu_{\uparrow,\downarrow}(E)$ is the density of states in the corresponding spin subband. Since the energy E lies below the bottom of $\varepsilon_{\downarrow}(\mathbf{k})$ spectrum we have $\nu_{\downarrow}(E) = 0$, which leads to the disappearance of $\delta T_{\mathbf{k}\mathbf{k}'}^{\uparrow\uparrow}$ and of the asymmetric scattering $\mathcal{J}_{\mathbf{k}\mathbf{k}'}^{\uparrow\uparrow} = 0$ correspondingly. Therefore the topological Hall effect is strongly suppressed in the regime $2E < \Delta, kr_0 \lesssim 1$.

B. Classical scattering and the adiabatic spin motion

In this section we derive the expressions for the total asymmetric rates $\mathcal{J}_{ss'}$ from Eq. 9 valid in the classical and adiabatic limits. In other words we assume that the scattering potential radius significantly exceeds the electron wavelength $kr_0 \gg 1$ and that the electron spin quantization axis is adiabatically co-aligned with local magnetization ($\lambda_a \gg 1$). In this case the scattering problem finds a rather elegant solution based on classical mechanics.

As a starting point we use Eq. 7 and express \mathcal{J}_{ss} for the spin conserving scattering channels (the spin-flip scattering is suppressed $\mathcal{J}_{\uparrow\downarrow} \approx 0$ in the adiabatic limit) via the spin-dependent differential scattering cross-sections $d\sigma_s/d\theta$:

$$\mathcal{J}_{ss} = \frac{p_s}{2\pi\hbar} \int_0^{2\pi} \frac{d\sigma_s}{d\theta} \sin\theta d\theta, \quad (21)$$

here θ is the scattering angle, $p_s = \hbar k_s$ is the spin-dependent momenta from Eq. 2. In the assumed approximation we are allowed to calculate $d\sigma_s/d\theta$ by accounting for the classical

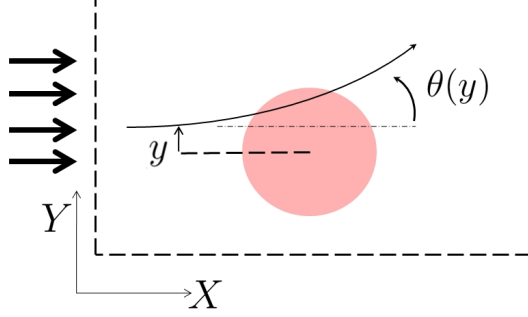


FIG. 2. The classical picture of an electron flux scattering.

trajectories of the electrons moving initially as a uniform incident beam, see Fig. 2. An electron approaching from the left boundary and having the impact parameter y is deflected by the scattering angle $\theta(y)$ being the function of y , the electron momentum \mathbf{p}_s after flying out of the scattering region has both projections $p_x^s = p_s \cos(\theta(y))$, $p_y^s = p_s \sin(\theta(y))$. We note that considering $\theta = \theta(y)$ in Eq. 21 as a function of the impact parameter and taking into account that $d\sigma_s/d\theta = dy(\theta)/d\theta$ one can rewrite the formula for \mathcal{J}_{ss} in the following way:

$$\mathcal{J}_{ss} = \frac{1}{2\pi\hbar} \int_{-\infty}^{\infty} p_y^s(y) dy, \quad (22)$$

which is now expressed only in terms of the transverse momentum projection $p_y^s(y)$ resulting from the classical trajectory with the impact parameter y .

The next step is to determine $p_y^s(y)$ which an electron gains moving inside a chiral potential. The condition of the adiabaticity indicates that the electron spin quantization axis rotates in space following the local direction of the magnetization $\mathbf{n}(\mathbf{r})$. During this process the electron wavefunction acquires a geometrical phase, which is the Berry phase when considered along a closed loop [49]. Essentially, it also manifests itself as the appearance of an effective magnetic field acting on the electron orbital motion [5, 8, 50]. This effect finds a classical explanation, which is described in details by Aharonov and Stern [51]. The equation of motion for an electron experiencing the adiabatic rotation of its spin axis is given:

$$\frac{d\mathbf{p}_s}{dt} = \frac{|e|\hbar}{c} [\mathbf{v} \times \mathbf{B}^s(\mathbf{r})] \quad (23)$$

here B_z^s is an effective spin-dependent magnetic field [8] which is responsible for the appearance of the topological Hall effect; it can be related to the geometrical characteristic of the

magnetization field, namely:

$$B_z^{\pm 1/2}(\mathbf{r}) = \pm \phi_0 \rho_{sk}(\mathbf{r}), \quad \rho_{sk}(\mathbf{r}) = \frac{1}{4\pi} \mathbf{n}(\mathbf{r}) \cdot [\partial_x \mathbf{n}(\mathbf{r}) \times \partial_y \mathbf{n}(\mathbf{r})]. \quad (24)$$

where $\phi_0 = hc/|e|$ is the magnetic flux quantum, and $\rho_{sk}(\mathbf{r})$ is the skyrmion density; we note that the unit vector in Eq. 24 obeys $\mathbf{n}_z(r \rightarrow \infty) = \mathbf{e}_z$, so the sign of ρ_{sk} is merely determined by χ . The total integral over ρ_{sk} gives the topological charge of a spin texture:

$$Q = \int \rho_{sk}(\mathbf{r}) d\mathbf{r} = 0, \pm 1, \pm 2 \dots, \quad (25)$$

the configurations having $Q \neq 0$ are classified as magnetic skyrmions [1]. Using Eq. 23 we express $p_y^s(y)$ in the following way:

$$p_y^s(y) = -\frac{|e|}{c} \int v_x(t) B_z^s(x(t), y(t)) dt, \quad (26)$$

where the integration goes over the time of the electron presence inside a scattering region, and $(x(t), y(t))$ is its classical trajectory. We further assume that the scattering has a small-angle character (it is typical for large scale potentials $kr_0 \gg 1$), i.e. the obtained transverse momentum $p_y^s \ll p_x^s$ is small compared to its initial value. At that one can further simplify the integration in Eq. 26 by replacing the coordinate $y(t)$ of the real trajectory by its initial position $y(t) \approx y$ and by imposing the integration $v_x(t) dt \approx dx$ over the straight line. The resulting expression for $p_y^s(y)$ is given:

$$p_y^s(y) = -\frac{|e|}{c} \int B_z^s(x(t), y) v_x(t) dt \approx -\frac{|e|}{c} \int_{-\infty}^{\infty} B_z^s(x, y) dx. \quad (27)$$

Finally, we substitute this formula into Eq. 22 and get for the total asymmetric rates:

$$\mathcal{J}_{\downarrow\downarrow} = -\mathcal{J}_{\uparrow\uparrow} = \int \rho_{sk}(\mathbf{r}) d\mathbf{r} = Q. \quad (28)$$

Thus we obtained a remarkable finding, namely \mathcal{J}_{ss} are entirely determined by the topological charge Q of a spin texture. The magnitude of the transverse current appears to be robust and independent of a particular distribution of magnetization inside a skyrmion core.

Let us emphasize, however, that the topological "quantization" does not have a universal character. Indeed, the result from Eq. 28 remains valid only upon three additional assumptions, namely the classical character of an electron motion, the small-angle character of the scattering and the adiabaticity of the electron spin motion. Apart from these assumptions

the topology of a spin texture ceases to be the unique requirement for the appearance of the scattering asymmetry. In particular, the expressions 12, 17 for $\mathcal{J}_{\mathbf{k}\mathbf{k}'}^{ss'}$ obtained via the perturbation theory do not reflect any topological features of a scattering potential; the asymmetric scattering takes place independently of Q in that case.

It is worth mentioning that the sign of the effective magnetic field B_z^s is opposite for two electron spin state, so the resulting asymmetry $\mathcal{J}_{\uparrow\uparrow} = -\mathcal{J}_{\downarrow\downarrow}$ in the adiabatic regime is spin-dependent which naturally leads to the spin Hall effect. This is in contrast to the behavior of the electron scattering on a pure spin texture in the weak coupling regime found in Eq. 17, when the scattering asymmetry is spin-independent.

The present consideration is equally applicable to the single subband case ($\Delta > 2E$). At sufficiently large potential radius the condition of adiabaticity becomes fulfilled as well, at that the Berry phase approach is also valid. Therefore we argue that the magnitude of the total asymmetric rate for the single subband regime will be also determined by Eq. 28.

IV. NUMERICAL SOLUTION (METHODS)

In this section we present the scheme for the numerical calculations of T -matrix describing the electron scattering on potentials from Eq. 3. The exact solution of the scattering problem is especially important for the investigation of the spin motion crossover which occurs when one passes from a perturbative scattering to the classical motion. The section has mostly a methodological character as it provides an alternative platform for the numerical studies of THE. The readers mainly interested in physical properties of the scattering can go straight to V, where the results obtained by the numerical calculations are discussed in details.

The considered potentials $V(\mathbf{r})$ have an important feature, namely the following commutator turns out to be zero:

$$[V(\mathbf{r}), -i\partial_\phi + \chi\hat{\sigma}_z/2] = 0. \quad (29)$$

The operator $-i\partial_\phi + \chi\hat{\sigma}_z/2$ has the meaning of z -component of the total angular momentum. The existence of such an integral of motion allows us to separate the polar coordinates $\mathbf{r} = (r, \phi)$ in the Schrodinger equation, which opens up a way towards the application of the phase theory of scattering. However, a specific angular structure of the associated eigenfunctions modifies the decomposition of T -matrix on its partial scattering parameters. The further consideration goes as follows. Firstly in IV B we derive the expansion of T -matrix

in terms of the eigenstates associated with $-i\partial_\phi + \chi\hat{\sigma}_z/2$, and secondly in [IV C](#) we adjust the phase-function method for the numerical calculations of the scattering parameters. The analysis given in sections [IV, V](#) is applicable for the case $E > \Delta/2$ when two spin subbands are activated. The single subband regime is considered separately in [V D](#).

A. Angular harmonics

The angular harmonics $\psi_m(\mathbf{r})$ corresponding to the operator $-i\partial_\phi + \chi\hat{\sigma}_z/2$ are given by:

$$\psi_m(r, \phi) = e^{im\phi} \begin{pmatrix} a_m(r) \\ e^{i(\chi\phi+\gamma)} b_m(r) \end{pmatrix}, \quad (30)$$

here $m = 0, \pm 1, \pm 2, \dots$ takes integer values, the functions a_m, b_m depend only on r . One can naturally see that ψ_m are the eigenfunctions of $-i\partial_\phi + \chi\sigma_z/2$ with the eigenvalue $m + \chi/2$. The functions $a_m(r), b_m(r)$ are determined by the explicit form of $v_{1,2}(r), u(r)$. The two-component functions $g_m \equiv (a_m, b_m)^T$ satisfy the following matrix equation:

$$\hat{\mathcal{H}}_m g_m(r) = -\omega_0 \hat{W}(r) g_m(r), \quad (31)$$

$$\hat{\mathcal{H}}_m = \begin{pmatrix} \frac{1}{r} \partial_r r \partial_r - \frac{m^2}{r^2} + k_\uparrow^2 & 0 \\ 0 & \frac{1}{r} \partial_r r \partial_r - \frac{(m+\chi)^2}{r^2} + k_\downarrow^2 \end{pmatrix}, \quad \hat{W}(r) = \begin{pmatrix} v_1(r) & u(r) \\ u(r) & v_2(r) \end{pmatrix},$$

where $\omega_0 = 2m_0 g / \hbar^2$ and we assume $E > \Delta/2$. Solving Eq. [31](#) gives us the relevant scattering parameters needed for the computation of T -matrix.

B. Decomposition of T -matrix

We note that the left part of Eq. [31](#) describes an electron free motion, so that away from the scattering potential $r > r_0$ the right side of Eq. [31](#) is absent and there are two independent cylindrical waves $g_m^{1,2}(r)$ given by:

$$g_m^1 = \begin{pmatrix} J_m(k_\uparrow r) - \mathcal{K}_m^{11} Y_m(k_\uparrow r) \\ -\mathcal{K}_m^{21} Y_{m+\chi}(k_\downarrow r) \end{pmatrix}, \quad g_m^2 = \begin{pmatrix} -\mathcal{K}_m^{12} Y_m(k_\uparrow r) \\ J_{m+\chi}(k_\downarrow r) - \mathcal{K}_m^{22} Y_{m+\chi}(k_\downarrow r) \end{pmatrix}, \quad (32)$$

where J_m, Y_m are the Bessel functions of the first and second kind respectively, the matrices $\hat{\mathcal{K}}_m$ of constant coefficients \mathcal{K}_m^{ij} ($i, j = 1, 2$) are determined by $\hat{W}(r)$ profile at $r < r_0$. Our goal is to express T -matrix through $\hat{\mathcal{K}}_m$ coefficients.

Let us consider a wave function $\Psi(\mathbf{r})$ which satisfies the full Eq. 1 with energy E and which has the following asymptotic form away from the scattering potential $r \gg r_0$:

$$\Psi(r, \varphi) = \psi_{in} + \psi_{sc},$$

$$\psi_{in} = \begin{pmatrix} e^{ik'_\uparrow r} u_\uparrow \\ e^{ik'_\downarrow r} u_\downarrow \end{pmatrix}, \quad \psi_{sc}(r, \varphi) = \frac{1}{\sqrt{r}} \begin{pmatrix} e^{ik_\uparrow r} (f_{\uparrow\uparrow} u_\uparrow + f_{\uparrow\downarrow} u_\downarrow) \\ e^{ik_\downarrow r} (f_{\downarrow\uparrow} u_\uparrow + f_{\downarrow\downarrow} u_\downarrow) \end{pmatrix}, \quad (33)$$

here $\mathbf{r} = (r, \varphi)$ is the radius vector in the polar coordinates, the function ψ_{in} describes the incident plane wave with energy E and momentum direction $\mathbf{n}' = (\cos \varphi', \sin \varphi')$, the magnitude of the wavevector differs for two spin subband $\mathbf{k}'_s = (k'_s, \varphi')$, where k'_s are given in Eq. 2, the polar angle φ' corresponds to the direction on the incident flux; the coefficients $u_{1,2}$ determine the incident spin polarization of the electron ($|u_1|^2 + |u_2|^2 = 1$). The second term ψ_{sc} corresponds to the outgoing cylindrical scattered wave, $f_{ss'}(\varphi, \varphi')$ is the scattering amplitude; here φ is regarded as the polar angle of the scattered plane wave described by the wavevectors $\mathbf{k}_s = (k_s, \varphi)$ so that the scattering angle is defined as $\theta = \varphi - \varphi'$. The scattering amplitude $f_{ss'}(\varphi, \varphi')$ is connected with T -matrix at the mass shell as [45]:

$$T_{\mathbf{k}\mathbf{k}'}^{ss'} = -\frac{\hbar^2}{m_0} \sqrt{\frac{2\pi k_s}{i}} f_{ss'}(\varphi, \varphi'). \quad (34)$$

We further decompose $\Psi(\mathbf{r})$ over the set of the angular harmonics ψ_m from Eq. 30:

$$\Psi(r, \varphi) = \sum_m i^m e^{-im\varphi'} (\mathcal{A}_m^1 \psi_m^1(\mathbf{r}) + \mathcal{A}_m^2 \psi_m^2(\mathbf{r})), \quad (35)$$

where $\mathcal{A}_m^{1,2}$ are some coefficients, and the functions $\psi_m^{1,2}$ taken at $r > r_0$ correspond to two linearly independent solutions $g_m^{1,2}(r)$ given by Eq. 32. The divergent and convergent parts of the full $\Psi = \Psi^+ + \Psi^-$ and the incident $\psi_{in} = \psi_{in}^+ + \psi_{in}^-$ wave functions at $r > r_0$ are given by:

$$\psi^\pm = \frac{1}{2} \sum_m i^m e^{im\theta} \begin{pmatrix} u_1 H_m^\pm(k_\uparrow r) \\ u_2 H_m^\pm(k_\downarrow r) \end{pmatrix}, \quad (36)$$

$$\Psi^\pm = \frac{1}{2} \sum_m i^m e^{im\theta} \left[\mathcal{A}_m^1 \begin{pmatrix} (1 \pm i\mathcal{K}_m^{11}) H_m^\pm(k_\uparrow r) \\ e^{i(\chi\theta + \bar{\gamma})} (\pm i\mathcal{K}_m^{21}) H_{m+\chi}^\pm(k_\downarrow r) \end{pmatrix} + \mathcal{A}_m^2 \begin{pmatrix} (\pm i\mathcal{K}_m^{12}) H_m^\pm(k_\uparrow r) \\ e^{i(\chi\theta + \bar{\gamma})} (1 \pm i\mathcal{K}_m^{22}) H_{m+\chi}^\pm(k_\downarrow r) \end{pmatrix} \right],$$

where $\bar{\gamma} = \gamma + \chi\varphi'$, and H_m^\pm are the Hankel functions of the first and second kind respectively. The scattered wave $\psi_{sc} = \Psi - \psi_{in}$ does not contain a convergent part, which brings us to

the following system of equations on $\mathcal{A}_m^{1,2}$:

$$\begin{pmatrix} 1 - i\mathcal{K}_m^{11} & -i\mathcal{K}_m^{12} \\ -i\mathcal{K}_m^{21} & 1 - i\mathcal{K}_m^{22} \end{pmatrix} \begin{pmatrix} \mathcal{A}_m^1 \\ \mathcal{A}_m^2 \end{pmatrix} = \begin{pmatrix} u_1 \\ u_2 e^{i\delta} \end{pmatrix}, \quad \delta = \pi\chi/2 - \bar{\gamma}. \quad (37)$$

The solutions of these equations are given by: $(\mathcal{A}_m^1, \mathcal{A}_m^2)^T = (\hat{I} - i\hat{\mathcal{K}}_m)^{-1} (u_1, u_2 e^{i\delta})^T$, where \hat{I} is the unit matrix 2×2 . Let us mention the appearance of an additional phase factor δ . The comparison of the scattered wave $\psi_{sc} = \Psi^+ - \psi_{in}^+$ in the asymptotic region for the Hankel function $H_m^+(x) \rightarrow (-i)^m e^{ix} \sqrt{(2/i\pi x)}$ with the expression for ψ_{sc} containing $f_{ss'}(\varphi, \varphi')$ leads us to the following expression for the scattering amplitude $f_{ss'}(\varphi, \varphi')$:

$$f_{ss'}(\varphi, \varphi') = \frac{1}{\sqrt{2\pi i}} \sum_m e^{im\theta} \begin{pmatrix} \frac{1}{\sqrt{k_\uparrow}} (S_m^{11} - 1) & \frac{1}{\sqrt{k_\uparrow}} S_m^{12} e^{-i(\chi\varphi' + \gamma')} \\ e^{i(\chi\varphi + \gamma')} \frac{1}{\sqrt{k_\downarrow}} S_m^{21} & e^{i\chi\theta} \frac{1}{\sqrt{k_\downarrow}} (S_m^{22} - 1) \end{pmatrix}_{ss'}, \quad (38)$$

where $\gamma' = \gamma - \pi\chi/2$ and we introduced the partial \hat{S}_m -matrices according to:

$$\hat{S}_m = (\hat{I} + i\hat{\mathcal{K}}_m) \cdot (\hat{I} - i\hat{\mathcal{K}}_m)^{-1}. \quad (39)$$

The present coupling between \hat{S}_m and $\hat{\mathcal{K}}_m$ is commonly known for multichannel scattering problems. Using the relation 34 we finally get the decomposition of T -matrix:

$$T_{\mathbf{k}\mathbf{k}'}^{ss'} = \frac{i}{2\pi\nu_0} \sum_m e^{im\theta} \begin{pmatrix} S_m^{11} - 1 & S_m^{12} e^{-i(\chi\varphi' + \gamma')} \\ S_m^{21} e^{i(\chi\varphi + \gamma')} & e^{i\chi\theta} (S_m^{22} - 1) \end{pmatrix}_{ss'}, \quad (40)$$

where the coefficients S_m^{ij} are determined by a particular spatial profile $\hat{W}(r)$.

C. Phase-function method

In this section we describe the numerical method for the calculation of $\hat{S}_m, \hat{\mathcal{K}}_m$ parameters entering in Eq. 40, 39. The Shrodinger equation is of the second order thus it requires two boundary conditions. In order to eliminate the necessity to address the wave function asymptotics at $r \gg r_0$ one uses the so-called phase function method [52, 53], which replaces the second order Eq. 31 by the first order nonlinear Cauchy problem for a set of scattering parameters. The Cauchy problem can be further solved using the standard computational software. Here we provide step by step derivation of this method purposely, so that one could straightforwardly adjust the similar calculations for more complex band structures.

Let us write Eq. 31 in the following form:

$$\left(\hat{\mathcal{H}}_m^0 + \hat{I}r^{-1}\partial_r r \partial_r\right)g_m(r) = -\omega_0 \hat{W}(r)g_m(r), \quad (41)$$

where $\hat{\mathcal{H}}_m^0 = \text{diag}(k_\uparrow^2 - m^2/r^2, k_\downarrow^2 - (m + \chi)^2/r^2)$ and \hat{I} is the unit matrix 2×2 . Following the textbook [52, 53] for a multichannel scattering we present the functions $g_m(r)$ as:

$$g_m(r) = \left(\hat{J}_m(r) - \hat{Y}_m(r)\hat{\mathcal{K}}_m(r)\right)\mathcal{C}_m(r), \quad (42)$$

$$\hat{J}_m(r) = \begin{pmatrix} J_m(k_\uparrow r) & 0 \\ 0 & J_{m+\chi}(k_\downarrow r) \end{pmatrix}, \quad \hat{Y}_m(r) = \begin{pmatrix} Y_m(k_\uparrow r) & 0 \\ 0 & Y_{m+\chi}(k_\downarrow r) \end{pmatrix},$$

where the 2×2 matrix $\hat{\mathcal{K}}_m(r)$ and the two-component column $\mathcal{C}_m(r)$ are some functions of the coordinate r . Outside the scattering region $r > r_0$ the functions $g_m(r)$ can be present in form 32 with the matrix of r -independent coefficients $\hat{\mathcal{K}}_m$; at that the normalization column \mathcal{C}_m will describe the polarization structure of an electron state. In order to endow $\hat{\mathcal{K}}_m(r)$ with the meaning of the real scattering parameters on the potential $\hat{W}(\tilde{r})\theta(r - \tilde{r})$ cut off at point $r < r_0$ one has to impose the additional condition for the derivative of g_m :

$$\frac{dg_m}{dr} = \left(\frac{d\hat{J}_m}{dr} - \frac{d\hat{Y}_m}{dr}\hat{\mathcal{K}}_m(r)\right)\mathcal{C}_m(r). \quad (43)$$

The matrices $\hat{\mathcal{K}}_m(r)$ satisfying both Eq. 41,43 and taken at the boundary point $\hat{\mathcal{K}}_m(r_0)$ will correspond to the real scattering parameters of a potential $\hat{W}(r)$. The introduced functions $\hat{\mathcal{K}}_m(r)$ are called the phase functions.

We further proceed with the derivation of the first order equation on $\hat{\mathcal{K}}_m(r)$. Let us substitute $g_m(r)$ in Eq. 41 and take into account the condition 43. The term containing only the second derivatives of g_m can be written as:

$$\begin{aligned} \frac{1}{r} \frac{d}{dr} r \frac{d}{dr} \left(\hat{J}_m - \hat{Y}_m \hat{\mathcal{K}}_m\right) \mathcal{C}_m &= \left[\left(\hat{J}_m'' + \hat{J}_m'/r\right) - \left(\hat{Y}_m'' + \hat{Y}_m'/r\right) \hat{\mathcal{K}}_m \right] \mathcal{C}_m + \\ &+ \left(\hat{J}_m' - \hat{Y}_m' \hat{\mathcal{K}}_m\right) \frac{d\mathcal{C}_m}{dr} - \hat{Y}_m' \frac{d\hat{\mathcal{K}}_m}{dr} \mathcal{C}_m. \end{aligned} \quad (44)$$

The terms in the square brackets from above cancel out $\hat{\mathcal{H}}_m^0 g_m$ term in Eq. 41, thus Eq. 41 does not contain the second derivatives:

$$\left(\hat{J}_m' - \hat{Y}_m' \hat{\mathcal{K}}_m\right) \frac{d\mathcal{C}_m}{dr} - \hat{Y}_m' \frac{d\hat{\mathcal{K}}_m}{dr} \mathcal{C}_m = -\omega_0 \hat{W}(r) \left(\hat{J}_m - \hat{Y}_m \hat{\mathcal{K}}_m\right) \mathcal{C}_m. \quad (45)$$

The next step is to express $d\mathcal{C}_m/dr$ through $d\hat{\mathcal{K}}_m/dr$. After multiplying this formula on $(\hat{J}_m - \hat{\mathcal{K}}_m \hat{Y}_m)$ we get for the left side of the equation:

$$\left(\hat{J}'_m - \hat{\mathcal{K}}_m \hat{Y}'_m\right) \left(\hat{J}_m - \hat{Y}_m \hat{\mathcal{K}}_m\right) \frac{d\mathcal{C}_m}{dr} - \left(\hat{J}_m - \hat{\mathcal{K}}_m \hat{Y}_m\right) \hat{Y}'_m \frac{d\hat{\mathcal{K}}_m}{dr} \mathcal{C}_m + \left[\hat{\mathcal{K}}_m, \hat{\mathcal{W}}_m\right] \frac{d\mathcal{C}_m}{dr}, \quad (46)$$

where $\hat{\mathcal{W}}_m = \hat{Y}'_m \hat{J}_m - \hat{Y}_m \hat{J}'_m$ is the Wronskian matrix of the Bessel functions and $\left[\hat{\mathcal{K}}_m, \hat{\mathcal{W}}_m\right]$ is the commutator of two matrices. Using the condition 43 one can further express $(\hat{J}_m - \hat{Y}_m \hat{\mathcal{K}}_m) \cdot d\mathcal{C}_m/dr$ through $d\hat{\mathcal{K}}_m/dr$, so Eq. 41 takes form:

$$-\hat{\mathcal{W}}_m \frac{d\hat{\mathcal{K}}_m}{dr} \mathcal{C}_m + \left[\hat{\mathcal{K}}_m, \hat{\mathcal{W}}_m\right] \frac{d\mathcal{C}_m}{dr} = -\omega_0 \left(\hat{J}_m - \hat{\mathcal{K}}_m \hat{Y}_m\right) \hat{W}(r) \left(\hat{J}_m - \hat{Y}_m \hat{\mathcal{K}}_m\right) \mathcal{C}_m. \quad (47)$$

Noting that $\left[\hat{\mathcal{K}}_m, \hat{\mathcal{W}}_m\right] = 0$ due to $\hat{\mathcal{W}}_m = \hat{I} \times (2/\pi r)$ we finally get the equation only in terms of $\hat{\mathcal{K}}_m(r)$ functions:

$$\frac{d\hat{\mathcal{K}}_m}{dr} = \frac{\pi r}{2} \omega_0 \left(\hat{J}_m - \hat{\mathcal{K}}_m \hat{Y}_m\right) \hat{W}(r) \left(\hat{J}_m - \hat{Y}_m \hat{\mathcal{K}}_m\right). \quad (48)$$

The initial condition is $\hat{\mathcal{K}}_m(0) = 0$. The scattering matrices \hat{S}_m can be further obtained by calculating this equation up to $r = r_0$ and using Eq. 39.

Alternatively, based on Eq. 48,39 one can derive the equation directly on $\hat{S}_m(r)$ functions. Introducing $S_m(r) \equiv (\hat{I} + i\hat{\mathcal{K}}_m(r)) \cdot (\hat{I} - i\hat{\mathcal{K}}_m(r))^{-1}$, the derivative of $\hat{\mathcal{K}}_m$ can be expressed as:

$$i \frac{d\hat{\mathcal{K}}_m}{dr} = \frac{d\hat{S}_m}{dr} (\hat{I} - i\hat{\mathcal{K}}_m) - i\hat{S}_m \frac{d\hat{\mathcal{K}}_m}{dr}.$$

After troublesome algebra Eq. 48 with the derivative from above is transformed to:

$$\frac{d\hat{S}_m(r)}{dr} = i \frac{\pi r}{4} \omega_0 \left(\hat{H}_m^- + \hat{S}_m \hat{H}_m^+\right) \hat{W}(r) \left(\hat{H}_m^- + \hat{H}_m^+ \hat{S}_m\right), \quad (49)$$

$$\hat{H}_m^\pm = \begin{pmatrix} H_m^\pm(k_\uparrow r) & 0 \\ 0 & H_{m+\chi}^\pm(k_\downarrow r) \end{pmatrix}, \quad \hat{W}(r) = \begin{pmatrix} v_1(r) & u(r) \\ u(r) & v_2(r) \end{pmatrix}.$$

The initial condition is $\hat{S}_m(0) = \hat{I}$. We note, that Eq. 49 is more convenient for numerical calculations than Eq. 48. Indeed, in case of a single channel scattering problem the parameter $\mathcal{K}_m = \tan \delta_m$ would correspond to the tangent of the partial scattering phase δ_m . When the potential radius is increased so are the scattering phases; particularly the latter can take value $|\delta_m| \rightarrow \pi/2$. At that $\mathcal{K}_m \rightarrow \infty$ diverges while $S_m = e^{2i\delta_m}$ remains finite. The analogous situation takes place for a multichannel scattering problem: when evaluating Eq. 48 the functions $\hat{\mathcal{K}}_m(r)$ can turn to the infinity at some points, while Eq. 49 and the functions $\hat{S}_m(r)$ are free of such negative feature.

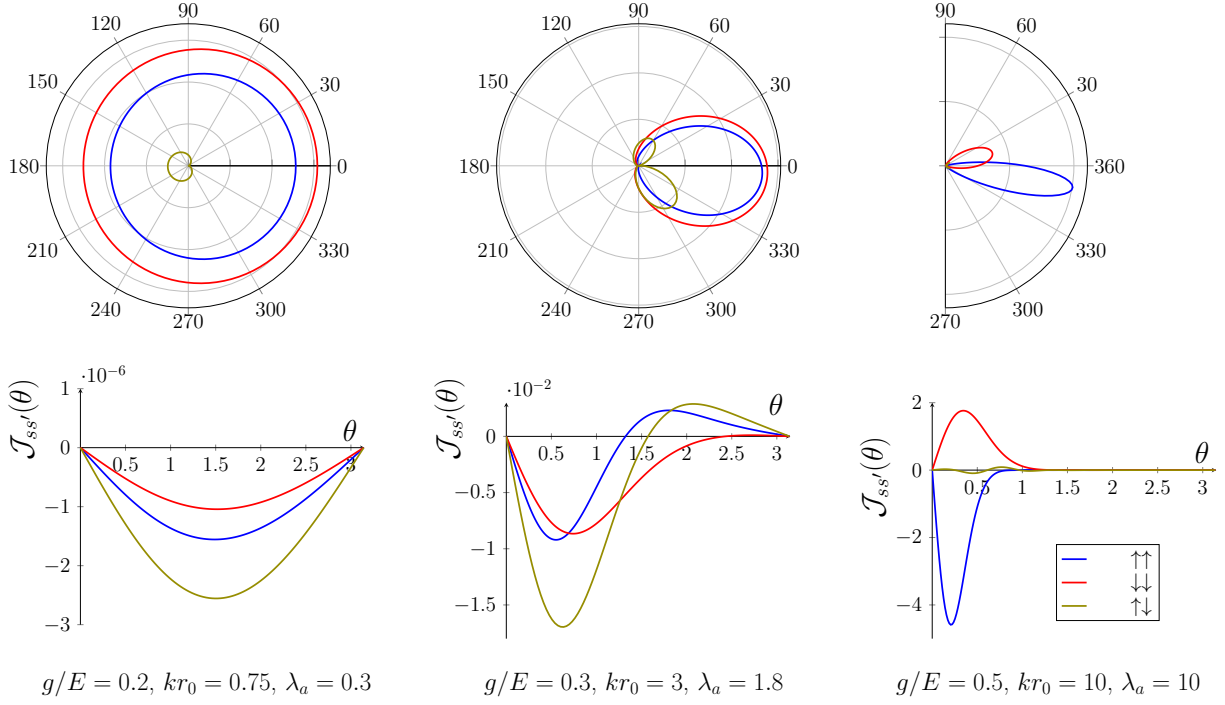


FIG. 3. The scattering pattern and the asymmetric scattering rates $\mathcal{J}_{ss'}(\theta) \equiv \mathcal{J}_{\mathbf{k}\mathbf{k}'}$.

V. NUMERICAL SOLUTION (RESULTS)

In this section we discuss the results for the scattering on chiral potentials obtained by the numerical calculations of Eq. 49.

A. Scattering on a magnetic skyrmion in different regimes

Here we consider the scattering on a magnetic skyrmion, namely we assume the following coupling between the scattering potential elements:

$$v_1(r) = -v_2(r) = n_z(r) - 1, \quad u(r) = n_{\parallel}(r), \quad n_{\parallel}^2(r) + n_z^2(r) = 1. \quad (50)$$

We parametrize the functions $n_z = \cos \Theta(r)$, $n_{\parallel} = \sin \Theta(r)$ using the azimuthal angle of the magnetization field $\Theta(r)$. The spin splitting of the electron subbands $\Delta = 2g$. In the calculations shown below we take $\chi = 1$ and make use of the following skyrmion profile:

$$\Theta(r) = \pi \left(1 - \frac{r}{r_0} \right), \quad r < r_0. \quad (51)$$

In Fig.3 we demonstrate the computed scattering pattern along with the θ -dependence of the asymmetric rates $\mathcal{J}_{ss'}(\theta) \equiv \mathcal{J}_{\mathbf{k}\mathbf{k}'^{ss'}}$ for different scattering regimes. The left panel corresponds to the weak-coupling regime. As we discussed in III A, the scattering within the spin-conserving channels indeed has an isotropic-like character, while the spin-flip channels are characterized by the suppression of the forward scattering. The asymmetric rates show a sin-like dependence on the scattering angle, the type of the scattering asymmetry is unique for all scattering channels, which is in full agreement with Eq. 17,18. The middle panel demonstrates the crossover regime, here the scattering pattern starts narrowing into the forward direction and the asymmetric rates gradually lose a certain preferable direction. The right panel shows the scattering in the adiabatic regime. The spin-flip scattering channels are suppressed in this case. The small-angle scattering taking place for the spin-conserving channels is featured by the pronounced spin-dependent asymmetry, the latter indicates the presence of the spin-dependent magnetic fields due to the Berry phase, see III B.

The symmetry crossover between the spin-dependent and the spin-independent Hall responses has been firstly discovered in [42]; the detailed discussion of its features can be found in [31]. Let us mention that to describe the behavior of the scattering rates in the crossover regime one necessarily has to address the exact solution of the scattering problem, at that the numerical scheme from IV is of special importance.

B. Classical limit and the topology

In III B we demonstrated that when both the classical and the adiabatic conditions are fulfilled ($kr_0, \lambda_a \gg 1$) the total asymmetric rates \mathcal{J}_{ss} are quantized with its magnitude determined by the topological charge Q of a magnetization field. Below this effect is examined by the numerical calculations. We consider two purely magnetic potentials featured by the different topology of parental spin textures. We take $\chi = 1$ and use the following spin texture profiles (the parametrization is introduced in Eq. 50, $\Delta = 2g$):

$$\begin{aligned}
 (Q = 1) \quad \Theta(r) &= \pi \left(1 - \frac{r}{r_0}\right), & r < r_0; \\
 (Q = 0) \quad \Theta(r) &= 2\pi \frac{r}{r_0} \left(1 - \frac{r}{r_0}\right), & r < r_0.
 \end{aligned}
 \tag{52}$$

In the right panel of Fig. 4 we demonstrate the computed dependence of \mathcal{J}_{ss} on the spin texture radius when entering into the classical and adiabatic limits ($g/E = 0.5$ is

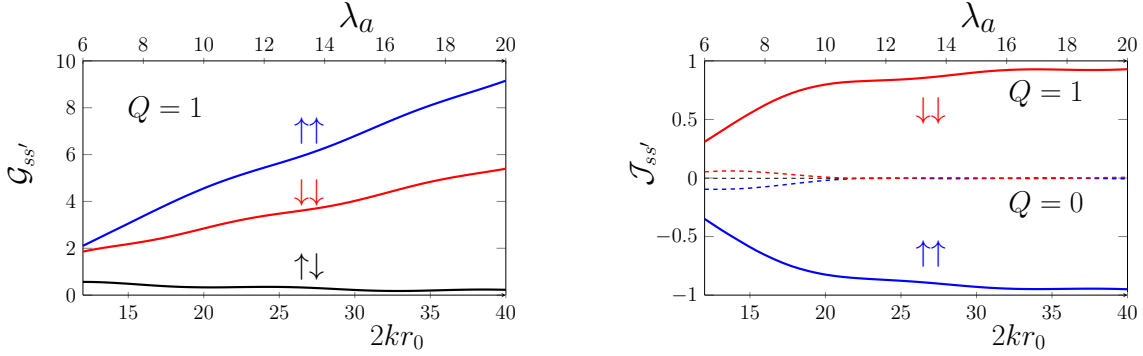


FIG. 4. The dependence of the total symmetric $\mathcal{G}_{ss'}$ and asymmetric $\mathcal{J}_{ss'}$ rates on the potential radius in units kr_0 for $Q = 0, 1$ spin configurations, the ratio $g/E = 0.5$.

fixed). This figure shows that there is a saturation of \mathcal{J}_{ss} when kr_0 increases, the limiting magnitude of $|\mathcal{J}_{ss}|$ approaches $Q = 1$ for the skyrmion configuration and goes down to zero for the topologically uncharged texture $Q = 0$. This is a clear manifestation of the topological features discussed in III B, namely the asymmetric rates approach the limiting values $\mathcal{J}_{\downarrow} = -\mathcal{J}_{\uparrow} = Q$ determined by the topology.

In the left panel of Fig. 4 we demonstrate the behavior of the average symmetric rate $\mathcal{G}_{ss'}$ for different scattering channels in the same region of parameters as for \mathcal{J}_{ss} ; here the data is present only for $Q = 1$ configuration. We note that the magnitude of $\mathcal{G}_{\uparrow\downarrow}$ for the spin-flip channel indeed gets suppressed when λ_a is increased, this is the consequence of the spin adiabaticity. It is worth mentioning that \mathcal{G}_{ss} for the spin-conserving channels increase linearly with the scatterer size, which is expected for a scattering in 2D systems. On the contrary, upon the increase of r_0 the asymmetric rates \mathcal{J}_{ss} become independent in the region $kr_0 \gg 1$ not only on a scattering potential size, but on its particular inner structure as well.

C. Scattering on electrically charged skyrmions

In this section we study the electron asymmetric scattering in case when a scalar potential is present additionally to a magnetic skyrmion. We make use of the following parametrization for the diagonal elements $v_{1,2}$:

$$v_1(r) = n_z(r) - 1 + \delta U(r), \quad v_2(r) = 1 - n_z(r) + \delta U(r), \quad (53)$$

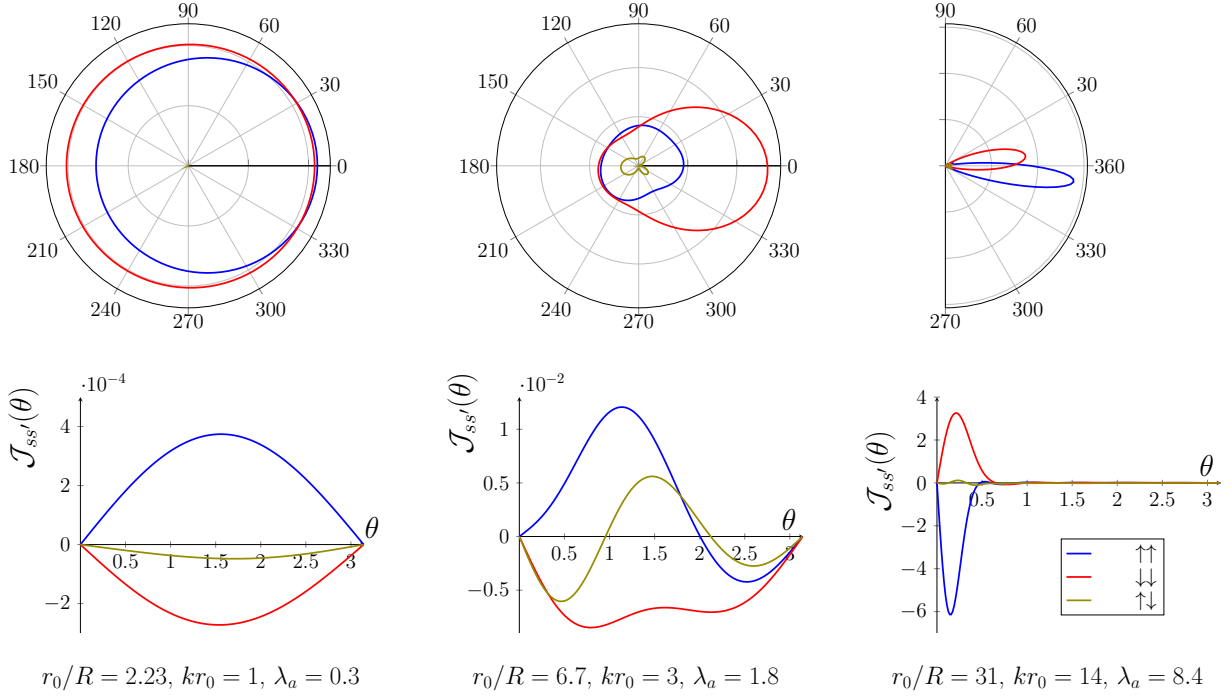


FIG. 5. The scattering pattern and the asymmetric scattering rates $\mathcal{J}_{ss'}(\theta) \equiv \mathcal{J}_{\mathbf{k}\mathbf{k}'}^{ss'}$ in case of an additional short-range scalar potential. The parameters: $U_0 = 30$, $kR = 0.45$, $g/E = 0.3$.

the off-diagonal component $u(r) = n_{\parallel}(r) = \sqrt{1 - n_z^2(r)}$ remains determined by $n_z(r)$, see Eq. 50. The subband splitting $\Delta = 2g$. For the numerical calculations we use the skyrmion profile from Eq. 51 and the following form of the potential $\delta U(r) = U_0 e^{-(r/R)^2}$ with R being its localization radius.

In Fig. 5 we demonstrate the scattering pattern and the θ -dependence of $\mathcal{J}_{\mathbf{k}\mathbf{k}'}^{ss'}$ for different skyrmion radii. In this plot only r_0 is varied, other parameters such as the localization radius R , scattering energy E and g, U_0 remain unchanged. The left panel of Fig. 5 corresponds to the perturbative scattering regime, here the scalar potential and the skyrmion are close in size. It is seen from the left panel that $\mathcal{J}_{\mathbf{k}\mathbf{k}'}^{\uparrow\uparrow}, \mathcal{J}_{\mathbf{k}\mathbf{k}'}^{\downarrow\downarrow}$ have different signs, which is consistent with the results of the weak coupling theory III A and Eq. 19 predicting that the nonmagnetic component of $V(\mathbf{r})$ restores the spin Hall effect and suppresses the spin-independent scattering caused by a pure magnetic texture. The right panel of Fig. 5 corresponds to the adiabatic regime with respect to the skyrmion size; here $\delta U(r)$ is kept localized ($r_0/R = 31$) so its length R is small compared to r_0 . The scattering rates in this regime have a similar structure to that in case of a pure magnetic skyrmion (see Fig. 3). Therefore in case of a large

skyrmion the short-range scalar perturbation does not affect significantly the asymmetric scattering, the latter is mainly produced during a lingering electron motion in the skyrmion texture surrounding $\delta U(r)$, at that the general arguments given in III B for the classical regime remain applicable. The middle panel in Fig. 5 corresponds to the intermediate case, here both the scattering pattern and $\mathcal{J}_{\mathbf{k}\mathbf{k}'}$ are strongly influenced by the presence of $\delta U(r)$. We note that the scattering asymmetry in the weak coupling regime depends on the sign of U_0 . Data shown in Fig. 5 is obtained for the positive value $U_0 = 30$, at that the scattering asymmetry for the spin up and the spin down states shown in the left panel differs from that in the classical limit. Increasing r_0 drives the scattering channels to switch their asymmetry, at that a complex scattering pattern at the intermediate region is indeed expected.

D. One spin subband regime

In this section we consider the case when $E < \Delta/2$ and only the spin up subband is available for a free motion (see Fig. 1). Firstly we adjust the phase function method for this regime and secondly we discuss some numerical results.

The following matrix equations on $g_m(r)$ functions should be used instead of Eq. 31:

$$\hat{\mathcal{H}}'_m g_m(r) = -\omega_0 \hat{W}(r) g_m(r), \quad (54)$$

$$\hat{\mathcal{H}}'_m = \begin{pmatrix} \frac{1}{r} \partial_r r \partial_r - \frac{m^2}{r^2} + k_\uparrow^2 & 0 \\ 0 & \frac{1}{r} \partial_r r \partial_r - \frac{(m+\chi)^2}{r^2} - \varkappa^2 \end{pmatrix}, \quad \hat{W}(r) = \begin{pmatrix} v_1(r) & u(r) \\ u(r) & v_2(r) \end{pmatrix},$$

where we introduced the real parameter $\varkappa = \sqrt{2m_0(\Delta/2 - E)}$. Two independent solutions $g_m^{1,2}$ of Eq. 54 away from the scattering potential $r > r_0$ are given by:

$$g_m^1 = \begin{pmatrix} J_m(k_\uparrow r) - \mathcal{K}_m^{11} Y_m(k_\uparrow r) \\ -\mathcal{K}_m^{21} K_{m+\chi}(\varkappa r) \end{pmatrix}, \quad g_m^2 = \begin{pmatrix} -\mathcal{K}_m^{12} Y_m(k_\uparrow r) \\ I_{m+\chi}(\varkappa r) - \mathcal{K}_m^{22} K_{m+\chi}(\varkappa r) \end{pmatrix}, \quad (55)$$

where I_m, K_m are modified Bessel functions of the first and second kind respectively. Among all \mathcal{K}_m^{ij} coefficients only $\mathcal{K}_m \equiv \mathcal{K}_m^{11}$ remains relevant for the scattering properties. Indeed, the asymptotic form of the propagating wavefunction at $r \gg r_0$ contains only spin-up state:

$$\Psi'(r, \varphi) = \left(e^{i\mathbf{k}'\mathbf{r}} + \frac{e^{ikr}}{\sqrt{r}} f(\varphi, \varphi') \right) | \uparrow \rangle. \quad (56)$$

Since I_m entering in $| \downarrow \rangle$ state diverges at $r \gg r_0$ the expansion of Ψ' over the partial harmonics $g_m^{1,2}$ cannot contain the admixture of g_m^2 functions. Therefore the scattering

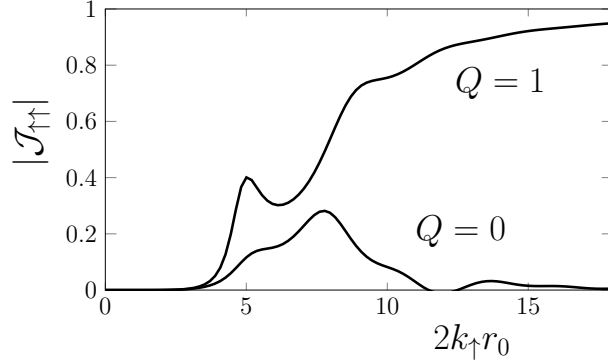


FIG. 6. The dependence of the total asymmetric rate $\mathcal{J}_{\uparrow\uparrow}$ on the potential radius in units kr_0 for $Q = 0, 1$ spin configurations, the ratio $g/E = 2.5$.

amplitude is given by a conventional single-channel decomposition:

$$f(\varphi, \varphi') = \frac{1}{\sqrt{2\pi ik_{\uparrow}}} \sum_m e^{im(\varphi - \varphi')} (\mathcal{S}_m - 1), \quad \mathcal{S}_m = \frac{1 + i\mathcal{K}_m}{1 - i\mathcal{K}_m}. \quad (57)$$

The phase-function method is adjusted for the one spin subband case using Eq. 54,55.

We introduce the phase functions $\hat{\mathcal{K}}_m(r)$ according to the following notation:

$$g_m(r) = \left(\hat{Q}_m - \hat{Z}_m \hat{\mathcal{K}}_m \right) \mathcal{C}_m(r), \quad \frac{dg_m}{dr} \equiv \left(\frac{d\hat{Q}_m}{dr} - \frac{d\hat{Z}_m}{dr} \hat{\mathcal{K}}_m \right) \mathcal{C}_m(r),$$

$$\hat{Q}_m(r) = \begin{pmatrix} J_m(k_{\uparrow}r) & 0 \\ 0 & \sqrt{\frac{2}{\pi}} I_{m+\chi}(\alpha r) \end{pmatrix}, \quad \hat{Z}_m(r) = \begin{pmatrix} Y_m(k_{\uparrow}r) & 0 \\ 0 & -\sqrt{\frac{2}{\pi}} K_{m+\chi}(\alpha r) \end{pmatrix}, \quad (58)$$

where the normalization constant $\sqrt{2/\pi}$ is introduced to make the Wronskian $\hat{Q}_m \hat{Z}'_m - \hat{Q}'_m \hat{Z}_m = \hat{I} \times 2/\pi r$ proportional to the unity matrix. Using the functions g_m from Eq. 58 and making the similar transformations of Eq. 54 as were described in IVC we get the following equations for $\hat{\mathcal{K}}_m(r)$ and $\hat{S}_m(r) = (\hat{I} + i\hat{\mathcal{K}}_m) \cdot (\hat{I} + i\hat{\mathcal{K}}_m)^{-1}$ matrix functions:

$$\frac{d\hat{\mathcal{K}}_m}{dr} = \frac{\pi r}{2} \omega_0 \left(\hat{Q}_m - \hat{\mathcal{K}}_m \hat{Z}_m \right) \hat{W}(r) \left(\hat{Q}_m - \hat{Z}_m \hat{\mathcal{K}}_m \right), \quad (59)$$

$$\frac{d\hat{S}_m}{dr} = i \frac{\pi r}{4} \omega_0 \left(\hat{Q}_m - i\hat{Z}_m + \hat{S}_m \cdot \left(\hat{Q}_m + i\hat{Z}_m \right) \right) \hat{W}(r) \left(\hat{Q}_m - i\hat{Z}_m + \left(\hat{Q}_m + i\hat{Z}_m \right) \cdot \hat{S}_m \right).$$

Let us mention that to calculate the scattering amplitude only $\mathcal{K}_m \equiv \mathcal{K}_m^{11}$ element of the whole matrix is needed.

We further apply this technique to study the scattering on a purely magnetic potential with the parametrization present in Eq. 50. In Fig. 6 we demonstrate the dependence

of the total asymmetric rate $\mathcal{J}_{\uparrow\uparrow}$ on the magnetic texture radius r_0 for two topologically different configurations (in Fig. 6 the absolute value $|\mathcal{J}_{\uparrow\uparrow}|$ is shown; $\mathcal{J}_{\uparrow\uparrow}$ remains negative in accordance with the previous considerations). Here we take $\chi = 1$ and use the spin texture profiles from Eq. 52, the subband spin splitting $\Delta = 2g$. As follows from our calculations $\mathcal{J}_{\uparrow\uparrow}$ gets strongly suppressed at small $kr_0 \lesssim 1$. This fact has been already mentioned in III A when considering the perturbative region: it is due to the vanishing of the third-order correlator in Eq. 20. We also notice that the asymptotic behavior of $\mathcal{J}_{\uparrow\uparrow}$ at $k_{\uparrow}r_0 \gg 1$ is similar to that observed for two opened spin subbands (see VB and Fig. 4). Namely, the asymmetric rate $\mathcal{J}_{\uparrow\uparrow} \rightarrow -1$ saturates for the topologically charged configuration $Q = 1$ while going to zero for the uncharged one $Q = 0$. This result stems from the Berry phase description III B valid for each subband independently. It is worth mentioning, however, that in the intermediate region when neither perturbative theory nor the Berry phase approach are valid the asymmetric scattering generally persists independently of a spin texture topology. As follows from Fig. 6 in the range of ($5 \lesssim 2k_{\uparrow}r_0 \lesssim 10$) the scattering rate $\mathcal{J}_{\uparrow\uparrow}$ has approximately the same magnitude for $Q = 0, 1$ configurations.

VI. CONCLUSIONS

To summarize, we have considered the asymmetric electron scattering on a skyrmion-like magnetic texture. We have obtained a number of analytical results valid in the limiting regimes of weak and strong coupling, we have also developed a numerical scheme allowing to quantify the Hall response for an arbitrary case. The present analysis has revealed that when the electron orbital and spin motions can be viewed classically the magnitude of the Hall current is determined by the topological charge of a magnetic texture. However, we argue that beyond these conditions the topology of a magnetization is not relevant for the appearance of the Hall response. In particular, we have shown that in the weak coupling regime the asymmetric scattering rates have the same angular structure independently of a scattering potential profile. We have also analyzed the behavior of the scattering pattern in case of an electrically charged skyrmion. The presence of a short-range impurity is mostly important in the nonadiabatic regime, at that the charge transverse response due to magnetic texture is superseded by the spin Hall effect.

ACKNOWLEDGMENTS

The Author thanks I.V. Rozhansky and N.S. Averkiev for helpful and fruitful discussions. The work has been carried out with the financial support of the Russian Science Foundation (project 18-72-10111). K.S.D. also thanks the Foundation for the Advancement of Theoretical Physics and Mathematics BASIS.

- [1] N. Nagaosa and Y. Tokura, [Nature Nanotechnology](#) **8**, 899 (2013).
- [2] X. Yu, W. Koshibae, Y. Tokunaga, K. Shibata, Y. Taguchi, N. Nagaosa, and Y. Tokura, [Nature](#) **564**, 95 (2018).
- [3] A. Fert, N. Reyren, and V. Cros, [Nature Reviews Materials](#) **2**, 17031 (2017).
- [4] R. Wiesendanger, [Nature Reviews Materials](#) **1**, 16044 (2016).
- [5] G. Sundaram and Q. Niu, [Phys. Rev. B](#) **59**, 14915 (1999).
- [6] C. Franz, F. Freimuth, A. Bauer, R. Ritz, C. Schnarr, C. Duvinage, T. Adams, S. Blügel, A. Rosch, Y. Mokrousov, and C. Pfleiderer, [Phys. Rev. Lett.](#) **112**, 186601 (2014).
- [7] P. M. Buhl, F. Freimuth, S. Blügel, and Y. Mokrousov, [Physica Status Solidi \(RRL\) - Rapid Research Letters](#) **11**, 1700007 (2017).
- [8] P. Bruno, V. K. Dugaev, and M. Taillefumier, [Phys. Rev. Lett.](#) **93**, 096806 (2004).
- [9] A. Neubauer, C. Pfleiderer, B. Binz, A. Rosch, R. Ritz, P. G. Niklowitz, and P. Böni, [Phys. Rev. Lett.](#) **102**, 186602 (2009).
- [10] M. Leroux, M. Stolt, S. Jin, D. Pete, C. Reichhardt, and B. Maiorov, [Scientific reports](#) **8**, 15510 (2018).
- [11] N. Kanazawa, Y. Onose, T. Arima, D. Okuyama, K. Ohoyama, S. Wakimoto, K. Kakurai, S. Ishiwata, and Y. Tokura, [Phys. Rev. Lett.](#) **106**, 156603 (2011).
- [12] C. Spencer, J. Gayles, N. Porter, S. Sugimoto, Z. Aslam, C. J. Kinane, T. R. Charlton, F. Freimuth, S. Chadov, S. Langridge, J. Sinova, C. Felser, S. Blügel, Y. Mokrousov, and C. H. Marrows, [Phys. Rev. B](#) **97**, 214406 (2018).
- [13] C. Moreau-Luchaire, C. Moutafis, N. Reyren, J. Sampaio, C. Vaz, N. Van Horne, K. Bouzehouane, K. Garcia, C. Deranlot, P. Warnicke, *et al.*, [Nature nanotechnology](#) **11**, 444 (2016).
- [14] W. Legrand, D. Maccariello, N. Reyren, K. Garcia, C. Moutafis, C. Moreau-Luchaire, S. Collin, K. Bouzehouane, V. Cros, and A. Fert, [Nano letters](#) **17**, 2703 (2017).

- [15] M. Raju, A. Yagil, A. Soumyanarayanan, A. Tan, A. Almoalem, F. Ma, O. Auslaender, and C. Panagopoulos, [Nature Communications](#) **10**, 696 (2019).
- [16] A. Soumyanarayanan, M. Raju, A. Oyarce, A. Tan, M.-Y. Im, A. P. Petrović, P. Ho, K. Khoo, M. Tran, C. Gan, *et al.*, [Nature materials](#) **16**, 898 (2017).
- [17] L. Wang, Q. Feng, Y. Kim, R. Kim, K. H. Lee, S. D. Pollard, Y. J. Shin, H. Zhou, W. Peng, D. Lee, *et al.*, [Nature Materials](#) **17**, 1087 (2018).
- [18] N. Romming, C. Hanneken, M. Menzel, J. Bickel, B. Wolter, K. von Bergmann, A. Kubetzka, and R. Wiesendanger, [Science](#) **341**, 636 (2013).
- [19] N. Romming, A. Kubetzka, C. Hanneken, K. von Bergmann, and R. Wiesendanger, [Phys. Rev. Lett.](#) **114**, 177203 (2015).
- [20] S. Meyer, M. Perini, S. von Malottki, A. Kubetzka, R. Wiesendanger, K. von Bergmann, and S. Heinze, [Nature Communications](#) **10**, 3823 (2019).
- [21] K. Zeissler, S. Finizio, K. Shahbazi, J. Massey, F. Al MaMari, D. M. Bracher, A. Kleibert, M. C. Rosamond, E. H. Linfield, T. A. Moore, *et al.*, [Nature nanotechnology](#) **13**, 1161 (2018).
- [22] N. Kanazawa, M. Kubota, A. Tsukazaki, Y. Kozuka, K. S. Takahashi, M. Kawasaki, M. Ichikawa, F. Kagawa, and Y. Tokura, [Phys. Rev. B](#) **91**, 041122 (2015).
- [23] D. Maccariello, W. Legrand, N. Reyren, K. Garcia, K. Bouzehouane, S. Collin, V. Cros, and A. Fert, [Nature Nanotechnology](#) , 1748 (2018).
- [24] Y. Ohuchi, Y. Kozuka, M. Uchida, K. Ueno, A. Tsukazaki, and M. Kawasaki, [Phys. Rev. B](#) **91**, 245115 (2015).
- [25] Y. Yun, Y. Ma, T. Su, W. Xing, Y. Chen, Y. Yao, R. Cai, W. Yuan, and W. Han, [Phys. Rev. Materials](#) **2**, 034201 (2018).
- [26] C. Liu, Y. Zang, W. Ruan, Y. Gong, K. He, X. Ma, Q.-K. Xue, and Y. Wang, [Phys. Rev. Lett.](#) **119**, 176809 (2017).
- [27] K. Karube, J. S. White, D. Morikawa, C. D. Dewhurst, R. Cubitt, A. Kikkawa, X. Yu, Y. Tokunaga, T.-h. Arima, H. M. Rønnow, *et al.*, [Science Advances](#) **4**, eaar7043 (2018).
- [28] K.-Y. Meng, A. S. Ahmed, M. Bac?ani, A.-O. Mandru, X. Zhao, N. Bague?s, B. D. Esser, J. Flores, D. W. McComb, H. J. Hug, *et al.*, [Nano Letters](#) **19**, 3169 (2019).
- [29] K. Nakazawa, M. Bibes, and H. Kohno, [Journal of the Physical Society of Japan](#) **87**, 033705 (2018).
- [30] K. Nakazawa and H. Kohno, [Phys. Rev. B](#) **99**, 174425 (2019).

- [31] K. S. Denisov, I. V. Rozhansky, N. S. Averkiev, and E. Lähderanta, [Phys. Rev. B **98**, 195439 \(2018\)](#).
- [32] H. Ishizuka and N. Nagaosa, [New Journal of Physics **20**, 123027 \(2018\)](#).
- [33] H. Ishizuka and N. Nagaosa, [Science Advances **4**, eaap9962 \(2018\)](#).
- [34] G. Metalidis and P. Bruno, [Phys. Rev. B **74**, 045327 \(2006\)](#).
- [35] M. Taillefumier, B. Canals, C. Lacroix, V. K. Dugaev, and P. Bruno, [Phys. Rev. B **74**, 085105 \(2006\)](#).
- [36] J.-i. Ohe, T. Ohtsuki, and B. Kramer, [Phys. Rev. B **75**, 245313 \(2007\)](#).
- [37] P. B. Ndiaye, C. A. Akosa, and A. Manchon, [Phys. Rev. B **95**, 064426 \(2017\)](#).
- [38] C. A. Akosa, H. Li, G. Tatara, and O. A. Tretiakov, [Phys. Rev. Applied **12**, 054032 \(2019\)](#).
- [39] K. Hamamoto, M. Ezawa, and N. Nagaosa, [Phys. Rev. B **92**, 115417 \(2015\)](#).
- [40] B. Göbel, A. Mook, J. Henk, and I. Mertig, [Phys. Rev. B **95**, 094413 \(2017\)](#).
- [41] B. Göbel, A. Mook, J. Henk, and I. Mertig, [The European Physical Journal B **91**, 179 \(2018\)](#).
- [42] K. S. Denisov, I. V. Rozhansky, N. S. Averkiev, and E. Lähderanta, [Scientific Reports **7**, 17204 \(2017\)](#).
- [43] Y. Araki and K. Nomura, [Phys. Rev. B **96**, 165303 \(2017\)](#).
- [44] K. S. Denisov, I. V. Rozhansky, N. S. Averkiev, and E. Lähderanta, [Phys. Rev. Lett. **117**, 027202 \(2016\)](#).
- [45] S. K. Adhikari, [American Journal of Physics **54**, 362 \(1986\)](#).
- [46] G. Tatara and H. Kawamura, [J. Phys. Soc. of Japan **71**, 2613 \(2002\)](#).
- [47] A. Lazuta, S. Maleyev, and B. Toperverg, [Physics Letters A **65**, 348 \(1978\)](#).
- [48] O. G. Udalov and A. A. Fraerman, [Phys. Rev. B **90**, 064202 \(2014\)](#).
- [49] M. V. Berry, [Proceedings of the Royal Society of London. A. Mathematical and Physical Sciences **392**, 45 \(1984\)](#).
- [50] J. Ye, Y. Kim, A. J. Millis, B. I. Shraiman, P. Majumdar, and Z. Tešanović, [Phys. Rev. Lett. **83**, 3737 \(1999\)](#).
- [51] Y. Aharonov and A. Stern, [Phys. Rev. Lett. **69**, 3593 \(1992\)](#).
- [52] V. V. Babikov, *Phase-function method in quantum mechanics* (Nauka, 1976).
- [53] V. V. Babikov, [Usp. Fiz. Nauk **92**, 3 \(1967\)](#).